Modern Physics Letters B
Vol. 28, No. 27 (2014) 1450213 (21 pages)

DOI: 10.1142/S0217984914502133



# Structural determination and physical properties of 4d transitional metal diborides by first-principles calculations

Chun Ying, Erjun Zhao*, Lin Lin and Qingyu Hou
*College of Science, Inner Mongolia University of Technology, Hohhot 010051, China*
* *ejzhao@yahoo.com*

Received 30 June 2014
Revised 8 September 2014
Accepted 16 September 2014
Published 17 October 2014



The structural determination, thermodynamic, mechanical, dynamic and electronic properties of 4d transitional metal diborides $MB_2$ (M = Y–Ag) are systematically investigated by first-principles within the density functional theory (DFT). For each diboride, five structures are considered, i.e. $AlB_2$-, $ReB_2$-, $OsB_2$-, $MoB_2$- and $WB_2$-type structures. The calculated lattice parameters are in good agreement with the previously theoretical and experimental studies. The formation enthalpy increases from $YB_2$ to $AgB_2$ in $AlB_2$-type structure (similar to $MoB_2$- and $WB_2$-type). While the formation enthalpy decreases from $YB_2$ to $MoB_2$, reached minimum value to $TcB_2$, and then increases gradually in $ReB_2$-type structure (similar to $OsB_2$-type), which is consistent with the results of the calculated density of states. The structural stability of these materials relates mainly on electronegative of metals, boron structure and bond characters. Among the considered structures, $TcB_2$–$ReB_2$ ($TcB_2$–$ReB_2$ represents $TcB_2$ in $ReB_2$-type structure, the same hereinafter) has the largest shear modulus (248 GPa), and is the hardest compound. The number of electrons transferred from metals to boron atoms and the calculated densities of states (DOS) indicate that each diboride is a complex mixture of metallic, ionic and covalent characteristics. Trends are discussed.

*Keywords*: Borides; first-principles theory; crystal structure; elasticity.

PACS Number(s): 77.48.Bw, 63.20.dk, 74.62.Bf, 62.20.D

## 1. Introduction

More attraction of transition-metal diborides is induced from their unique properties such as high hardness, high melting point, chemical stability, good electrical–thermal conductivity and superconductivity.[1,2] Based on their well-known properties, these materials have been widely applied for cutting and grinding tools, abrasive resistance coating and mechanical process, etc. Therefore, extensive experimental and theoretical studies on structural, elastic, dynamic and electronic properties of transition-metal diborides have been performed very important for both fundamental and technological fields.

For 5d transition-metal diborides, the well-defined transition-metal diboride $ReB_2$ has been synthesized successfully at ambient pressure and had an average hardness of 48 GPa under an applied load of 0.49 N.[3] The structural, electronic and mechanical properties of $ReB_2$ have been studied systematically both from experiments and theories.[4–8] At the same time, investigations focused on $WB_2$ and $OsB_2$ have been performed by using first-principles calculations within both the generalized gradient approximation (GGA) and local density approximation (LDA), and the estimated hardness of $WB_2$ was very close to that of superhard $ReB_2$.[8] These studies yield hints for the design of superhard and ultra-incompressible materials of transition-metal diborides. Moreover, the 4d transition metals combining with small and covalent-bond-forming boron atoms are promising to create superhard and superconductive materials because of the high valence electron densities and the strong covalent bonding in these compounds.[9] Up to date, several of 4d transition-metal diborides $MB_2$ (M = Y,[10] Zr,[11] Mo,[12] Ru,[13] Ag[14]) have been synthesized by diverse methods. For 4d transition-metal diborides, the geometrical structure is assumed to be influenced by the electron transferred from neighboring metal atoms to the boron atoms. Elements with lower (higher) electronegativity (compared to boron) would donate (attract) electrons to neighboring atoms and favor to create planar (puckered) structure.[15] This has been confirmed that boron structure in $MB_2$ (M = Zr, Nb and Mo) is planar and others like $MB_2$ (M = Tc, Mo, Ru, Rh and Pd) favor to create puckered structure with highly directional covalency zigzag topology of inter connected bonds.[9] The structural, elastic and electronic properties of 4d transition-metal diborides $MB_2$ (M = Zr, Nb, Tc, Mo, Ru and Rh) have been investigated by using the first-principles calculations.[16] It was found that the ground state phases for $MB_2$ are hexagonal $AlB_2$-type ($ZrB_2$, $NbB_2$), hexagonal $ReB_2$-type ($TcB_2$, $RhB_2$), and orthorhombic ($MoB_2$, $RuB_2$).[16] The phonon dispersion and the thermodynamic properties of $ZrB_2$, $NbB_2$ and $MoB_2$ have been investigated by using the first-principles, and there was not very strong electron–phonon interaction in these compounds based on their calculation results.[17] For $ZrB_2$ with $AlB_2$-type structure, the band structure and the density of states (DOS) have been performed by using an augmented plane wave (APW) method and the band structure of $ZrB_2$ was determined by the $sp^2$ hybridization.[18,19] Band structure of $ZrB_2$ calculated by Johnson[19] was quite similar to the results obtained by Ihara[18] using the Korringa–Kohn–Rostoker (KKR) method in the spherical muffin-tin approximation. After then, the electronic structures, elasticity and hardness for $ZrB_2$ have been investigated by using first-principles total-energy plane-wave pseudopotential and the results suggested that $ZrB_2$ is almost isotropy in compression and in shear.[20] The strong hybridization of boron $2p$ and metal 4d states not only created the "pseudogap", but generated inter-layer covalent bonding.[20] Their calculated hardness for $ZrB_2$ was 23.16 GPa, which was in good agreement with experimental data ($23 \pm 0.9$ GPa).[20] For $MoB_2$, the structural and mechanical properties of $MoB_2$ with $SR_4$ structure (R-3m, $Z = 6$) have been performed at ambient pressure using the DFT within GGA, and the calculated results indicated that the strong covalent

bonding between Mo and B atoms is the driving force for the high bulk modulus (310 GPa) and shear modulus (238 GPa).[21] Most recently, the hardness, bulk modulus and shear modulus of the synthesized $MoB_2$ were about 21, 296 and 196 GPa, respectively.[12] For $RuB_2$, the electronic and structure properties with orthorhombic (space group Pmmm, No. 59) structure have been investigated by using the LDA, the results indicated that the high bulk modulus (about 334 GPa) is the result of covalent bonding between transition metal 4d and boron $2p$ states.[22] It was in good agreement with Wang's results using the DFT.[23] The elastic, structural and thermodynamic properties of $RuB_2$ with orthorhombic structure have been studied under high pressures by using the Vanderbilit-type nonlocal ultra-soft pseudopotentials (USP) with GGA.[24] Finally, for $AgB_2$, Islam *et al.*[25] has found the superconductivity at 7.4 K by using the density function perturbation theory (DFPT) within GGA. The structural and mechanical properties of $AgB_2$ have been investigated by using Vienna *ab initio* simulation package (VASP), and their calculated results suggested that $AgB_2$ is mechanically stable and elastically anisotropic in $AlB_2$-type structure, and becomes more ductile nature with the pressure increasing.[26]

In this present study, two structures ($AlB_2$- and $ReB_2$-type) are considered, because most of the ground state structures for 5d transitional metal diborides were $AlB_2$- and $ReB_2$-types.[27] Moreover, $WB_2$-, $MoB_2$- and $OsB_2$-type structures are also considered based on the chemically related compounds. However, much less is known about the mechanical properties of 4d transition metal diborides in these structures, especially for $MoB_2$- and $WB_2$-type structures. Motivated by above mentioned, the structural stability and physical properties of 4d transition metal diborides from $YB_2$ to $AgB_2$ are systematically studied by first-principles based on the DFT. The general trends are discussed.

## 2. The Computational Details and Crystal Structures

All the calculations are performed within the CASTEP code,[28] based on the density-functional theory. The generalized gradient approximation (GGA) parametrized by Perdew, Burk and Ernzerhof (PBE)[29] is used for the exchange-correlation potentials. The ultra-soft pseudopotentials (USP) are used to describe the interaction between the ions and the electrons.[30] The plane wave cut-off energy is chosen to be 450 eV. The $k$-point of $12 \times 12 \times 9$ for $AlB_2$-, $14 \times 14 \times 4$ for $ReB_2$-, $8 \times 13 \times 9$ for $OsB_2$-, $12 \times 12 \times 2$ for $MoB_2$- and $16 \times 16 \times 3$ for $WB_2$-type structures are generated using the Monkhorst–Pack scheme.[13] The structures are relaxed with respect to both lattice parameters and atomic position. The structural relaxations are performed until the difference in the total energy and the residual forces are less than $1.0 \times 10^{-6}$ eV and $1.0 \times 10^{-3}$ eV/Å, respectively. The elastic stiffness constants are calculated by using stress–strain method. The bulk modulus ($B$), shear modulus ($G$) and Young's modulus ($E$) are calculated from Viogt–Reuss–Hill approximation.[31–33] The formation enthalpy is calculated from $\Delta H = E\ (MB_2) - E$ (solid M) $-2E$ (solid B). In addition, the strength of covalent bond within M–B bonds is

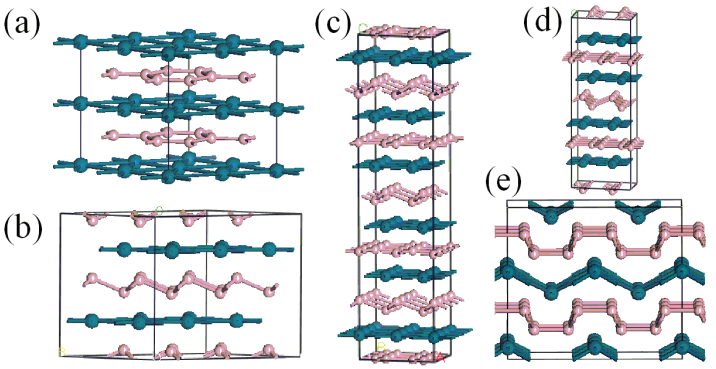


Fig. 1. (Color online) Crystal structures of $MB_2$ (M = Y to Ag): (a) $AlB_2$-type, (b) $ReB_2$-type, (c) $MoB_2$-type, (d) $WB_2$-type and (e) $OsB_2$-type structure. The large and small spheres represent 4d transition metal and boron atoms, respectively.



estimated by calculating the bond populations. The changes in atomic charge and bond populations are then calculated by projecting the plane wave states onto the localized basis set by means of Mulliken analysis.[9]

The considered crystal structures are plotted in Fig. 1. The simple planar (the form of boron layer) $AlB_2$-type (space group P6/mmm, No. 191), puckered (boron sheet) $ReB_2$-type (space group $P6_3/mmc$, No. 194),[34] puckered $OsB_2$-type (space group Pmmn, No. 59), planar-puckered $MoB_2$-type (space group R-3m, No. 166) and $WB_2$-type (space group $P6_3/mmc$, No. 194) structures are considered as initiating structures for 4d transition-metal diborides $MB_2$ (M = Y–Ag). In $AlB_2$-type structure, it contains only one formula unit with the M atom at site 1a $(0, 0, 0)$, and the B atom at 2d (1/3, 2/3, 1/2). Each M atom, located at the center of the hexagonal prism, is coordinated by twelve B atoms [Fig. 1(a)]. $ReB_2$-type structure [Fig. 1(b)] contains two formula units with the M atom at site 2c (1/3, 2/3, 1/4), while the B atom at site 4f (1/3, 2/3, 0.548). The B atoms are seven-fold coordinated with four M and three B atoms. Each M atom is coordinated by eight B atoms and locates at the center of a trigonal bipyramid.[4] $MoB_2$-type structure [Fig. 1(c)] contains six formula units with the M atom at site 6c $(0, 0, 0.075)$, while two B atoms at sites 6c $(0, 0, 0.332)$ and 6c $(0, 0, 0.182)$, respectively. In this structure, the B layers between the M layers form two kinds of hexagonal networks: One is a planar graphic-like layer and is sandwiched between the same M layers, similar to the packing of boron in $AlB_2$_type structure. Another one is more densely puckered sheet sitting between different M layers, similar to that in $ReB_2$-type. $WB_2$-type structure [Fig. 1(d)] contains four formula units with the M atom at site 4f (1/3, 2/3, 0.1376), while the three B atoms at sites 2b (0, 0, 1/4), 2d (1/3, 2/3, 3/4) and 4f (1/3, 2/3, 0.9757). $OsB_2$-type structure [Fig. 1(e)] contains two formula units with the M atom at site 2a (0, 0, 0.1535), while the B atom at site 4f (0.805, 0, 0.632). In this type, the M and B sheets are puckered.

Table 1. Calculated formation enthalpy per formula unit $\Delta H$ (eV), lattice parameters $a, c$ (Å), elastic constants $C_{ij}$ (GPa), bulk modulus $B$ (GPa), shear modulus $G$ (GPa), Young's modulus $E$ (GPa), Poisson's ratio $\nu$ and Debye temperature $\Theta_D$ (K) for the diborides in a hexagonal $AlB_2$-type structure with space group P6/mmm.

| | $YB_2$ | $ZrB_2$ | $NbB_2$ | $MoB_2$ | $TcB_2$ | $RuB_2$ | $RhB_2$ | $PdB_2$ | $AgB_2$ |
|---|---|---|---|---|---|---|---|---|---|
| $\Delta H$ | −1.26 | −3.18 | −2.32 | −1.02 | −0.03 | 0.34 | 0.12 | 0.76 | 1.45 |
| $a$ | 3.329 | 3.166 | 3.100 | 3.091 | 2.959 | 3.017 | 3.084 | 3.026 | 3.011 |
| | 3.303[a] | 3.151[d] | 3.084[c] | 3.000[c] | 2.940[c] | | | | 3.070[b] |
| | | 3.165[e] | 3.133[d] | 3.034[d] | | | | | 3.023[g] |
| $c$ | 3.917 | 3.540 | 3.331 | 3.330 | 3.399 | 3.269 | 3.247 | 3.594 | 4.077 |
| | 3.843[a] | 3.420[d] | 3.319[c] | 3.321[c] | 3.384[c] | | | | 3.810[b] |
| | | 3.547[e] | 3.237[d] | 3.245[d] | | | | | 4.080[g] |
| $C_{11}$ | 356 | 569 | 583 | 617 | 589 | 423 | 465 | | 99 |
| | | 569,[c] 568[f] | | 627[c] | 617[c] | | | | |
| $C_{33}$ | 342 | 445 | 446 | 462 | 529 | 433 | 379 | | 193 |
| | | 449,[c] 436[f] | | 398[c] | 550[c] | | | | |
| $C_{44}$ | 159 | 248 | 204 | 136 | 47 | 24 | 25 | | −15 |
| | | 262,[c] 247[f] | | 174[c] | 72[c] | | | | |
| $C_{12}$ | 71 | 53 | 125 | 132 | 181 | 270 | 214 | | 366 |
| | | 64,[c] 57[f] | | 120[c] | 178[c] | | | | |
| $C_{13}$ | 89 | 116 | 182 | 195 | 154 | 186 | 174 | | 72 |
| | | 122,[c] 120[f] | | 231[c] | 156[c] | | | | |
| $B$ | 172 | 239 | 287 | 304 | 298 | 284 | 268 | | |
| | | 240,[f] 245[c] | | 313[c] | 307[c] | | | | |
| $G$ | 145 | 235 | 200 | 175 | 114 | 55 | 66 | | |
| | | 231,[f] 241[c] | | 291[c] | 159[c] | | | | |
| $E$ | 340 | 530 | 486 | 441 | 304 | 155 | 185 | | |
| | | 526[f] | | | | | | | |
| $B/G$ | 1.19 | 1.02 | 1.44 | 1.73 | 2.60 | 5.16 | 4.04 | | |
| $\nu$ | 0.171 | 0.130 | 0.218 | 0.258 | 0.330 | 0.409 | 0.386 | | 0.643 |
| | | 0.135[f] | | | | | | | |
| $\Theta_D$ | 770 | 933 | 847 | 779 | 628 | 435 | 476 | | |
| | | 942[e] | | | | | | | |

[a]Ref. 10, Exp., [b]Ref. 14, Exp., [c]Ref. 16, GGA, [d]Ref. 17, GGA, [e]Ref. 20, GGA, [f]Ref. 38, Exp., [g]Ref. 25, GGA.

## 3. Results and Discussion

### 3.1. *$AlB_2$-type structure*

From Table 1, it is clear that $ZrB_2$–$AlB_2$ ($ZrB_2$–$AlB_2$ represents $ZrB_2$ in $AlB_2$-type structure, the same hereinafter) has the smallest formation enthalpy (−3.18 eV), following $NbB_2$–$AlB_2$ to about −2.32 eV. The calculated formation enthalpies for $MB_2$ from $YB_2$ to $TcB_2$ are negative, indicating that these diborides might be synthesized easily by experiments. This is confirmed by the synthesis of $YB_2$,[10] $ZrB_2$,[11] $NbB_2$ (Ref. 35) and $MoB_2$ (Ref. 36) in $AlB_2$-type structure. However, $TcB_2$–$AlB_2$ is not reported by experiment, which might be due to that $TcB_2$–$AlB_2$ (−0.03 eV) is thermodynamically unstable with respect to $TcB_2$–$ReB_2$ (−1.45 eV). Moreover,

the calculated phonon dispersion curves indicate that $MoB_2$–$ReB_2$ is dynamically stable, while $MoB_2$–$AlB_2$ is dynamically unstable due to the imaginary phonon frequency (see details in Fig. A.1 in Supplementary Materials). Others from $RuB_2$ to $AgB_2$ have positive formation enthalpies, implying that these compounds may be synthesized under extreme conditions, such as high temperature and/or high pressure. For $YB_2$, the lattice parameters 3.329 Å and 3.917 Å match the experimental values 3.303 Å and 3.843 Å,[10] deviating by about 0.8% for $a$-axis and 2.0% for $c$-axis. The calculated lattice parameters of $ZrB_2$ ($a = 3.166$ Å and $c = 3.540$ Å) are quite close to the values of previous studies ($a = 3.151$ Å and $c = 3.420$ Å in Ref. 17, and $a = 3.165$ Å and $c = 3.547$ Å in Ref. 20). For $NbB_2$, the lattice parameters 3.100 Å and 3.331 Å are in good agreement with the other calculated results by using GGA-PBE method.[16,17] For $MoB_2$, the lattice parameters 3.091 Å and 3.330 Å are consistent with the previously values (3.000 Å and 3.321 Å in Ref. 16) and (3.034 Å and 3.245 Å in Ref. 17). Our calculated values are in good agreement with experimental[16] and previously theoretical[14] studies for $TcB_2$ and $AgB_2$. They match each other within 1.8% for $a$-axis and 2.5% for $c$-axis.

The elastic stability is a necessary condition for a crystal to exist. From the mechanical stable criteria,[37] all the diborides with $AlB_2$-type except $AgB_2$, are elastically stable at ambient pressure (Table 1). $AgB_2$ is elastically unstable due to negative $C_{44}$ value (−15 GPa). From Table 1, it is interesting to note that $MoB_2$ has the highest $C_{11}$ value of 617 GPa, which deviates by around 1.6% from the previously theoretical value 627 GPa.[16] Our calculated $C_{33}$ value (462 GPa) of $MoB_2$ is in agreement with previously theoretical data (398 GPa).[16] For $TcB_2$, the calculated $C_{11}$ and $C_{33}$ values are 589 GPa and 529 GPa, which is slightly smaller than the previously theoretical values 617 GPa and 550 GPa,[16] deviating by 4.8% and 4.0%, respectively.

The Young's modulus and Poisson's ratio are two important factors, which are necessary to develop the technological and engineering applications of a material. It is obvious to see that $ZrB_2$–$AlB_2$ has the highest Young's modulus of 530 GPa, which is in excellent agreement with experimental data (526 GPa).[38] It is well known that higher Debye temperature corresponds to higher hardness. For instance, diamond has the highest Debye temperature of 2230 K, and it is the hardest material up to date. $ZrB_2$–$AlB_2$ has the highest Debye temperature (933 K) and is the hardest materials among the 4d transitional metal diborides with $AlB_2$-type structure. In addition, from Table 1, the calculated $B/G$ ratios for $MB_2$ (M = Y, Zr, Nb and Mo) indicate that they are brittle in nature because their values are less than 1.75, which is the critical value to separate ductility and brittleness.[39]

### 3.2. *$ReB_2$-type structure*

From Table 2, the calculated formation enthalpies for the diborides from $ZrB_2$ to $RhB_2$ in $ReB_2$-type structure are negative. Also, the calculated formation enthalpies gradually decrease from $YB_2$ (0.86 eV) to $TcB_2$ (−1.45 eV) in the $ReB_2$-type

Table 2. Calculated formation enthalpy per formula unit $\Delta H$ (eV), lattice parameters $a, c$ (Å), elastic constants $C_{ij}$ (GPa), bulk modulus $B$ (GPa), shear modulus $G$ (GPa), Young's modulus $E$ (GPa), Poisson's ratio $\nu$ and Debye temperature $\Theta_D$ (K) for the diborides in a hexagonal $ReB_2$-type structure with space group $P6_3/mmc$.

| | $YB_2$ | $ZrB_2$ | $NbB_2$ | $MoB_2$ | $TcB_2$ | $RuB_2$ | $RhB_2$ | $PdB_2$ | $AgB_2$ |
|---|---|---|---|---|---|---|---|---|---|
| $\Delta H$ | 0.86 | −0.55 | −0.83 | −1.16 | −1.45 | −0.94 | −0.42 | 0.52 | 1.16 |
| $a$ | 3.197 | 3.077 | 2.994 | 2.920 | 2.893 | 2.913 | 2.994 | 2.960 | 2.989 |
| | | | | 2.906[a] | 2.878[a] | 2.895[a] | 2.963[a] | | |
| $c$ | 9.542 | 8.539 | 8.058 | 7.739 | 7.444 | 7.271 | 7.259 | 7.664 | 8.688 |
| | | | | 7.700[a] | 7.470[a] | 7.242[a] | 7.156[a] | | |
| $C_{11}$ | 226 | 147 | 322 | 495 | 581 | 493 | 369 | 261 | |
| | | | | 531[a] | 608[a] | 467[a] | 361[a] | | |
| $C_{33}$ | 455 | 460 | 630 | 848 | 960 | 807 | 642 | 419 | |
| | | | | 876[a] | 947[a] | 813[a] | 718[a] | | |
| $C_{44}$ | 12 | 63 | 129 | 246 | 251 | 206 | 127 | 38 | |
| | | | | 247[a] | 256[a] | 209[a] | 137[a] | | |
| $C_{12}$ | 144 | 244 | 212 | 190 | 185 | 220 | 199 | 228 | |
| | | | | 178[a] | 136[a] | 178[a] | 231[a] | | |
| $C_{13}$ | 90 | 70 | 91 | 86 | 108 | 166 | 177 | 95 | |
| | | | | 88[a] | 111[a] | 161[a] | 205[a] | | |
| $B$ | 169 | 167 | 226 | 281 | 320 | 317 | 270 | 92 | |
| | | | | 294[a] | 320[a] | 305[a] | 302[a] | | |
| $G$ | 37 | | 105 | 217 | 248 | 185 | 117 | 22 | |
| | | | | 240[a] | 270[a] | 196[a] | 121[a] | | |
| $E$ | 103 | | 273 | 517 | 591 | 465 | 307 | 61 | |
| $B/G$ | 4.57 | | 2.15 | 1.30 | 1.29 | 1.71 | 2.31 | 4.22 | |
| $\nu$ | 0.398 | | 0.299 | 0.194 | 0.193 | 0.256 | 0.311 | 0.390 | |
| $\Theta_D$ | 406 | | 633 | 873 | 916 | 787 | 634 | 273 | |

[a]Ref. 16, GGA.

structure. While the formation enthalpies for $YB_2$ and $AgB_2$ are positive, implying that their synthesis might be more difficult, e.g. extreme temperature and/or extreme pressure. Therefore, up to date, only $TcB_2$ has been synthesized among the 4d transition-metal diborides in $ReB_2$-type structure.[40] For $MoB_2$, the calculated lattice parameters 2.920 Å and 7.739 Å are consistent with the previous theoretical values (2.906 Å and 7.700 Å).[16] For $TcB_2$, the calculated lattice parameters 2.893 Å and 7.444 Å deviate by around 0.5% for $a$-axis and 0.3% for $c$-axis compared with the previously theoretical data 2.878 Å and 7.470 Å.[16] An excellent agreement between our calculation and previous study[16] for the lattice parameters is also obtained for $RuB_2$ and $RhB_2$. As shown in Table 2, we find high incompressibility along the $c$-axis, as demonstrated by the large $C_{33}$ values. Among all the diborides in the considered structures, $TcB_2$ has the highest $C_{33}$ value of 960 GPa, which is consistent with the previously theoretical value 947 GPa,[16] matching within 1.4%. For $MoB_2$, it has the second large $C_{33}$ value of 848 GPa, followed by 807 GPa for $RuB_2$. This is in general agreement with previous studies.[16] Well known to us, the elastic moduli are the most important factors for identifying the hardness of solids.

It has been suggested that a linear correlation might exist between the shear modulus and Vickers hardness.[41] The calculated shear moduli are 217 GPa for $MoB_2$, 248 GPa for $TcB_2$ and 185 GPa for $RuB_2$ in $ReB_2$-type structure, which might have high hardness. So, according to the Chen's model,[42] the estimated Vickers hardness are 32.2 GPa for $MoB_2$, 13.0 GPa for $RuB_2$, and 35.1 GPa for $TcB_2$, which is in agreement with the previously theoretical values (43.3 GPa in Ref. 16 and 37.0 GPa in Ref. 17) for $TcB_2$. In addition, these compounds are brittle in nature associated with small $B/G$ values (Table 2), which are less than 1.75.

### 3.3. *$OsB_2$-type structure*

Each diborides in both $ReB_2$- and $OsB_2$-type structures exhibits similar formation enthalpies (Tables 2 and 3). Only $TcB_2$–$OsB_2$ has higher formation enthalpy (−1.29 eV) than that (−1.45 eV) of $TcB_2$–$ReB_2$. The calculated lattice parameters 4.641 Å, 2.911 Å and 4.225 Å of $MoB_2$–$OsB_2$ are quite close to previously theoretical values of 4.616 Å, 2.897 Å and 4.210 Å, deviating by around 0.5% in $a$-axis, 0.5% in $b$-axis, and 0.3% in $c$-axis.[16] For $RuB_2$–$OsB_2$, the calculated lattice parameters ($a$ = 4.647 Å, $b$ = 2.869 Å and $c$ = 4.046 Å) are in excellent agreement with theoretical ($a$ = 4.647 Å, $b$ = 2.869 Å, $c$ = 4.046 Å in Ref. 24) and experimental values ($a$ = 4.645 Å, $b$ = 2.865 Å and $c$ = 4.045 Å in Ref. 43). An agreement between our calculation and previous studies for the lattice parameters is also obtained for $MoB_2$ and $RhB_2$ with $OsB_2$-type structure (Table 3). Among the diborides in $OsB_2$-type structure, $TcB_2$ has the highest $C_{33}$ value of 816 GPa, which is consistent with the previously theoretical value 833 GPa, matching within 2.1%. For $MoB_2$, it has the second large $C_{33}$ value of 800 GPa, followed by 699 GPa for $RuB_2$ (Table 3). This is in agreement with previous studies.[16,24] The calculated shear moduli are 222 GPa for $MoB_2$, 232 GPa for $TcB_2$ and 183 GPa for $RuB_2$ with $OsB_2$-type structure, which are in agreement with the previously theoretical studies[16,24] with a maximum deviation of $\sim$5.2% (Table 3). In addition, $MB_2$ (M = Mo, Tc and Ru) are brittle associated with small $B/G$ values less than 1.75, while $MB_2$ (M = Rh, Pd and Ag) are ductile in nature (Table 3).

### 3.4. *$MoB_2$- and $WB_2$-type structures*

Each diboride with $MoB_2$- and $WB_2$-type structures has similar behave (Tables 4 and 5). It is interesting to note that $MoB_2$ is more favored to crystallize in these two structures, because they have the same formation enthalpy (−1.47 eV), which is the smallest value among the considered structures [Fig. 2(d)]. This is also confirmed by that only $MoB_2$ has been synthesized in $MoB_2$-type structure among the 4d transition-metal diborides.[44] $MoB_2$–$MoB_2$ has high $C_{33}$ value (624 GPa), which is close to that of 674 GPa for $MoB_2$–$WB_2$ (Tables 4 and 5). $MoB_2$–$MoB_2$ also has high shear modulus of 216 GPa (of 223 GPa in $MoB_2$–$WB_2$), which is in agreement with experimental value of 190 GPa.[12] According to our calculated results, $NbB_2$–$MoB_2$ also exhibits relatively high $C_{33}$ value of 596 GPa (of 609 GPa for $NbB_2$–

Table 3. Calculated formation enthalpy per formula unit $\Delta H$ (eV), lattice parameters $a, b, c$ (Å), elastic constants $C_{ij}$ (GPa), bulk modulus $B$ (GPa), shear modulus $G$ (GPa), Young's modulus $E$ (GPa), Poisson's ratio $\nu$ and Debye temperature $\Theta_D$ (K) for the diborides in a hexagonal $OsB_2$-type structure with space group Pmmn.

| | $YB_2$ | $ZrB_2$ | $NbB_2$ | $MoB_2$ | $TcB_2$ | $RuB_2$ | $RhB_2$ | $PdB_2$ | $AgB_2$ |
|---|---|---|---|---|---|---|---|---|---|
| $\Delta H$ | 0.96 | −0.40 | −0.85 | −1.18 | −1.29 | −0.97 | −0.36 | 0.53 | 1.49 |
| $a$ | 5.395 | 5.052 | 4.831 | 4.641 | 4.597 | 4.647 | 4.639 | 4.928 | 5.587 |
| | | | | 4.616[a] | 4.572[a] | 4.625,[a] 4.647,[b] 4.645[c] | 4.612[a] | | |
| $b$ | 3.107 | 3.075 | 2.997 | 2.911 | 2.883 | 2.869 | 2.995 | 2.799 | 2.730 |
| | | | | 2.897[a] | 2.869[a] | 2.874,[a] 2.869,[b] 2.865[c] | 2.944[a] | | |
| $c$ | 5.075 | 4.606 | 4.376 | 4.225 | 4.102 | 4.046 | 4.082 | 4.191 | 4.439 |
| | | | | 4.210[a] | 4.080[a] | 4.031,[a] 4.046,[b] 4.045[c] | 4.029[a] | | |
| $C_{11}$ | 219 | 251 | 464 | 471 | 535 | 535 | 372 | 342 | 342 |
| | | | | 472[a] | 534[a] | 544,[a] 525[b] | 404[a] | | |
| $C_{22}$ | 126 | 257 | 374 | 506 | 550 | 462 | 287 | 288 | 281 |
| | | | | 513[a] | 540[a] | 485,[a] 455[b] | 336[a] | | |
| $C_{33}$ | 253 | 361 | 571 | 800 | 816 | 699 | 535 | 438 | 293 |
| | | | | 818[a] | 833[a] | 718,[a] 698[b] | 608[a] | | |
| $C_{44}$ | −12 | −114 | −41 | 179 | 188 | 122 | 82 | 44 | 1.5 |
| | | | | 162[a] | 193[a] | 113,[a] 122[b] | 87[a] | | |
| $C_{55}$ | 35 | 85 | 201 | 294 | 267 | 225 | 119 | 23 | 27 |
| | | | | 303[a] | 305[a] | 227,[a] 216[b] | 116[a] | | |
| $C_{66}$ | 81 | 35 | 170 | 225 | 219 | 183 | 111 | 123 | 114 |
| | | | | 242[a] | 228[a] | 184,[a] 178[b] | 118[a] | | |
| $C_{12}$ | 100 | 93 | 161 | 192 | 154 | 180 | 239 | 171 | 110 |
| | | | | 211[a] | 186[a] | 177,[a] 171[b] | 237[a] | | |
| $C_{13}$ | 53 | 79 | 108 | 140 | 129 | 151 | 182 | 148 | 60 |
| | | | | 143[a] | 145[a] | 153,[a] 146[b] | 183[a] | | |
| $C_{23}$ | 38 | 100 | 87 | 64 | 75 | 108 | 137 | 117 | 23 |
| | | | | 60[a] | 90[a] | 119,[a] 117[b] | 129[a] | | |
| $B$ | 104 | 155 | 234 | 282 | 288 | 283 | 250 | 213 | 142 |
| | | | | 292[a] | 305[a] | 294,[a] 280[b] | 272,[a] 334[b] | | |
| $G$ | | | | 222 | 232 | 183 | 95 | 66 | 41 |
| | | | | 234[a] | 244[a] | 191,[a] 180[b] | 117[a] | | |
| $E$ | | | | 549 | 549 | 452 | 252 | 180 | 114 |
| $B/G$ | | | | 1.27 | 1.24 | 1.55 | 2.63 | 3.22 | 3.64 |
| $\nu$ | | | | 0.189 | 0.182 | 0.234 | 0.331 | 0.359 | 0.366 |
| $\Theta_D$ | | | | 771 | 775 | 682 | 498 | 409 | 335 |

[a]Ref. 16, GGA, [b]Ref. 24, GGA, [c]Ref. 43, Exp.

$WB_2$), high shear modulus of 211 GPa (of 219 GPa for $NbB_2$–$WB_2$) and high Debye temperature of 1108 K (of 923 K for $NbB_2$–$WB_2$).

The values of estimated Vickers hardness are 33.6 GPa, 30.0 GPa and 31.4 GPa for $MoB_2$ with $OsB_2$-, $MoB_2$- and $WB_2$-type, respectively, and 35.5 GPa for $TcB_2$ with $OsB_2$-type. This implies that $MoB_2$ ($ReB_2$-, $OsB_2$-, $MoB_2$- and $WB_2$-type), $TcB_2$ ($ReB_2$- and $OsB_2$-type), $ZrB_2$ ($AlB_2$-type), $NbB_2$ ($AlB_2$-, $MoB_2$- and $WB_2$-type) are the candidates of potential ultra-incompressible and superhard materials.

Table 4. Calculated formation enthalpy per formula unit $\Delta H$ (eV), lattice parameters $a, c$ (Å), elastic constants $C_{ij}$ (GPa), bulk modulus $B$ (GPa), shear modulus $G$ (GPa), Young's modulus $E$ (GPa), Poisson's ratio $\nu$ and Debye temperature $\Theta_D$ (K) for the diborides in a hexagonal $MoB_2$-type structure with space group R-3m.

| | $YB_2$ | $ZrB_2$ | $NbB_2$ | $MoB_2$ | $TcB_2$ | $RuB_2$ | $RhB_2$ | $PdB_2$ | $AgB_2$ |
|---|---|---|---|---|---|---|---|---|---|
| $\Delta H$ | 0.29 | −1.85 | −2.09 | −1.47 | −0.96 | −0.20 | −0.19 | 0.38 | 1.52 |
| $a$ | 3.273 | 3.154 | 3.059 | 3.011<br>3.015,[a] 3.016[b] | 2.973 | 2.943 | 2.988 | 3.006 | 3.003 |
| $c$ | 26.066 | 23.294 | 21.968 | 20.948<br>20.971,[a] 20.995[b] | 20.734 | 21.334 | 21.936 | 21.989 | 25.217 |
| $C_{11}$ | | 354 | 513 | 550 | 523 | 392 | 305 | 364 | |
| $C_{33}$ | | 447 | 596 | 624 | 572 | 346 | 304 | 306 | |
| $C_{44}$ | | 89 | 226 | 230 | 174 | −89 | −13 | 23 | |
| $C_{12}$ | | 108 | 110 | 126 | 139 | 225 | 227 | 133 | |
| $C_{13}$ | | 102 | 130 | 180 | 208 | 207 | 142 | 125 | |
| $C_{14}$ | | −11 | 31 | 17 | 9 | 4 | 15 | 16 | |
| $C_{15}$ | | 0 | 0 | 0 | 0 | 0 | 0 | 0 | |
| $B$ | | 196 | 262 | 298<br>295[b] | 301 | 266 | 214 | 200 | |
| $G$ | | | 211 | 216<br>190[b] | 178 | | | 57 | |
| $E$ | | | 500 | 522 | 446 | | | 158 | |
| $B/G$ | | | 1.24 | 1.38 | 1.69 | | | 3.51 | |
| $\nu$ | | | 0.181 | 0.208 | 0.253 | | | 0.367 | |
| $\Theta_D$ | | | 1108 | 1092 | 982 | | | 556 | |

[a]Ref. 43, Exp., [b]Ref. 12, Exp.

Table 5. Calculated formation enthalpy per formula unit $\Delta H$ (eV), lattice parameters $a, c$ (Å), elastic constants $C_{ij}$ (GPa), bulk modulus $B$ (GPa), shear modulus $G$ (GPa), Young's modulus $E$ (GPa), Poisson's ratio $\nu$ and Debye temperature $\Theta_D$ (K) for the diborides in a hexagonal $WB_2$-type structure with space group $P6_3/mmc$.

| | $YB_2$ | $ZrB_2$ | $NbB_2$ | $MoB_2$ | $TcB_2$ | $RuB_2$ | $RhB_2$ | $PdB_2$ | $AgB_2$ |
|---|---|---|---|---|---|---|---|---|---|
| $\Delta H$ | −0.292 | −1.83 | −2.08 | −1.47 | −0.91 | −0.16 | −0.17 | 0.40 | 1.53 |
| $a$ | 3.273 | 3.149 | 3.053 | 3.014 | 2.973 | 2.955 | 2.980 | 3.005 | 3.005 |
| $c$ | 17.379 | 15.567 | 14.662 | 13.945 | 13.838 | 14.146 | 14.742 | 14.696 | 16.790 |
| $C_{11}$ | | 388 | 526 | 571 | 544 | | 260 | 324 | |
| $C_{33}$ | | 472 | 609 | 674 | 570 | | 315 | 334 | |
| $C_{44}$ | | 98 | 233 | 221 | 151 | | −13 | 11 | |
| $C_{12}$ | | 89 | 117 | 132 | 146 | | 285 | 173 | |
| $C_{13}$ | | 94 | 127 | 160 | 183 | | 130 | 148 | |
| $B$ | | 199 | 266 | 301 | 297 | | 212 | 213 | |
| $G$ | | 130 | 219 | 223 | 175 | | | 39 | |
| $E$ | | 320 | 516 | 536 | 439 | | | 108 | |
| $B/G$ | | 1.53 | 1.21 | 1.35 | 1.70 | | | 5.46 | |
| $\nu$ | | 0.232 | 0.176 | 0.202 | 0.254 | | | 0.415 | |
| $\Theta_D$ | | 783 | 923 | 969 | 851 | | | 398 | |

Table 6. The calculated universal anisotropic factor $A^U$, shear anisotropic factors $A_1$, $A_2$, $A_3$, percentage anisotropy in compressibility $A_B$ (%) and shear $A_G$ (%) for $MoB_2$ and $TcB_2$ with considered structures.

| | $A^U$ | $A_1$ | $A_2$ | $A_3$ | $A_B$ | $A_G$ |
|---|---|---|---|---|---|---|
| | $MoB_2$ with different structures | | | | | |
| $AlB_2$-type | 0.394 | 0.786 | | 0.559 | 0.003 | 0.037 |
| $ReB_2$-type | 0.541 | 0.839 | | 1.614 | 0.011 | 0.049 |
| $OsB_2$-type | 0.491 | 0.722 | 0.998 | 1.517 | 0.101 | 0.044 |
| $MoB_2$-type | 0.058 | 1.130 | | 1.000 | 0.005 | 0.004 |
| $WB_2$-type | 0.020 | 0.955 | | 1.006 | 0.004 | 0.001 |
| | $TcB_2$ with different structures | | | | | |
| $AlB_2$-type | 3.047 | 0.233 | | 0.231 | 0.002 | 0.233 |
| $ReB_2$-type | 0.329 | 0.758 | | 1.269 | 0.013 | 0.029 |
| $OsB_2$-type | 0.250 | 0.688 | 0.878 | 1.127 | 0.010 | 0.022 |
| $MoB_2$-type | 0.052 | 1.025 | | 1.000 | 0.005 | 0.004 |
| $WB_2$-type | 0.084 | 0.807 | | 0.758 | 0.001 | 0.008 |



While $RuB_2$ ($ReB_2$- and $OsB_2$-type) might be just a hard material, because they have lower shear moduli than the compounds mentioned above (Tables 1–5). All the elastically stable 4d transition-metal diborides in the considered structures are likely to resist more volume change than shape change, because the calculated values of $B/G$ are larger than one (Tables 1–5).

It is well known that the elastic anisotropy is still important to understand the microcracks in solid state materials. A number of metrics, including the universal anisotropic index, percent anisotropy and shear anisotropic factors are listed in Table 6 for $MoB_2$ and $TcB_2$, which are studied due to their high elastic moduli and thermodynamic stability (seen in Tables 1–5). The universal anisotropic index $A^U$ and percent anisotropies ($A_B$ and $A_G$) have been defined in previous studies.[45,46] According to the formulas of shear anisotropy factors $A_1$ ($A_1 = A_2$) and $A_3$,[46] there is nearly the same anisotropy in $MoB_2$- and $WB_2$-type structure, which might be due to their similar layer structures (Fig. 1). Moreover, there is less anisotropy in $MoB_2$- and $WB_2$-type structures than those in $ReB_2$-, $OsB_2$- and $AlB_2$-type ones. This indicates that the orderly stacking of the metal layers, boron planar layers and boron puckered sheets makes the structure tend to isotropy. From Table 6, it is interesting to note that it is almost isotropy in compressibility and in shear for $MoB_2$- and $WB_2$-type structures.

### 3.5. *Trends of bonding properties*

From Fig. 2(a), it is clear that the cell volume of $ReB_2$-type $MB_2$ decreases from $YB_2$ and reaches minimum at $RuB_2$, and then increases. This trend is similar to those of other structures. While the mass density increases gradually from $YB_2$ and reaches maximum at $RuB_2$, and then decreases [Fig. 2(b)].

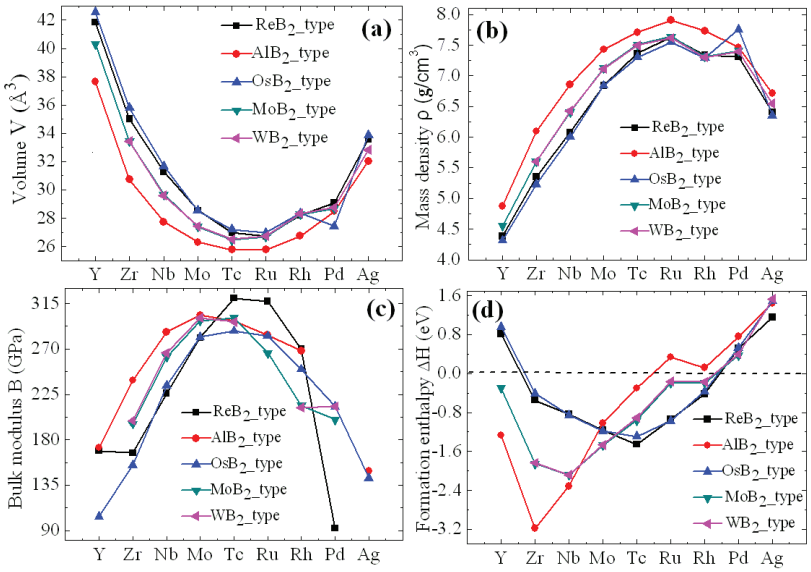


Fig. 2. (Color online) The calculated (a) volume $V$ (Å$^3$), (b) mass density $\rho$ (g/cm$^3$), (c) bulk modulus $B$ (GPa) and (d) formation enthalpy $\Delta H$ (eV) for all the considered $MB_2$ (M = Y to Ag).

The formation enthalpies for the considered structures are shown in Fig. 2(d). The general trend of formation enthalpy increases from $YB_2$ to $AgB_2$ (one exception for $ZrB_2$) in $AlB_2$-type structure. Similar trend is also observed in 4d transitional metal mononitrides.[2] However, the different trend of formation enthalpy is observed in $ReB_2$-type structure. The formation enthalpy decreases from $YB_2$ to $TcB_2$, and then increases gradually from $TcB_2$ to $AgB_2$ (the same trend is also found in $OsB_2$-type structure), which can be explained by the calculated densities of states (DOS), seen the later section in detail. Moreover, the formation enthalpies of diborides with $MoB_2$- and $WB_2$-type are located in the middle of those with $AlB_2$- and of $ReB_2$-type structures [Fig. 2(d)]. From Fig. 3, it is clear that there is a wide and deep valley, called as "pseudogap", which separates the bonding and antibonding states. For $YB_2$, the Fermi level is located at the left of the valley, indicating that not all the bonding states are occupied. From $YB_2$ to $TcB_2$, the bonding state is gradually occupied with the increase of valence electrons, which is in good agreement with the least formation enthalpy of $TcB_2$. For $RuB_2$, it can be seen from Fig. 3(f) that the valence electrons begin to occupy the antibonding states, which makes $ReB_2$-type $RuB_2$ energetically unfavorable. The DOS for the other compounds are given in the Supplementary Materials (Fig. A.2). Due to the finite DOS at the Fermi energy level, all the considered structures in the 4d transitional metal diborides are metallic.

At zero temperature, a stable crystalline structure requires all phonon frequencies to be positive. Therefore, the phonon dispersion curves are calculated for the

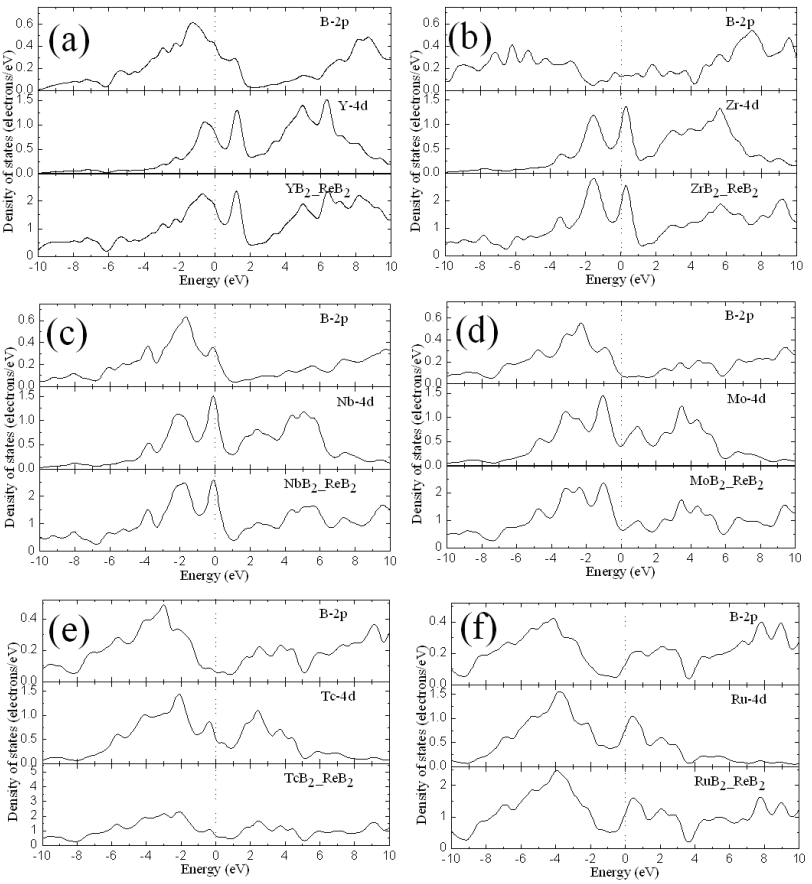


Fig. 3. The calculated partial and total densities of states for $MB_2$ (M = Y–Ru) in $ReB_2$-type structure. The vertical dotted line at zero indicates the Fermi energy level.

most stable $MB_2$ (M = Y to Ag) among the considered structures at ambient pressure and shown in Fig. 4. It is clearly seen that no imaginary phonon frequency is detected in the whole Brillouin zone for $MB_2$ (M = Y to Pd), implying their dynamical stability. While $AgB_2$–$ReB_2$ is dynamically unstable, due to the imaginary frequencies in the Brillouin zone. Due to $RhB_2$, $PdB_2$ and $AgB_2$ without any experiments, we should investigate their dynamic properties. For example, $RhB_2$ in all the considered structures, except the most stable $RhB_2$–$ReB_2$, have imaginary frequencies and thus are dynamically unstable, seen in Fig. A.3 in Supplementary Materials.

An obtained deeper knowledge concerning the underlying causes to the formation of planar or puckered $MB_2$ structure is, hence, important for future designing and development of new ultra-incompressible and superhard materials. The number of electrons transferred from the transition-metal atoms to neighboring boron

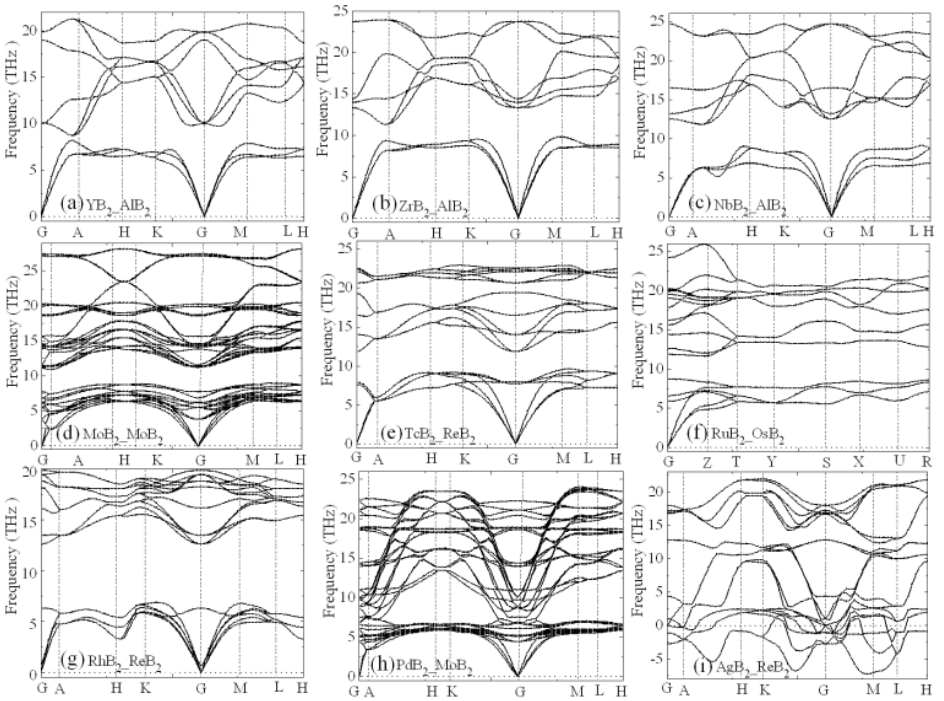


Fig. 4. The calculated phonon dispersions for $MB_2$ (M = Y to Ag) in the most stable structures.

atoms is listed in Table 7. From boron structure point of view, $MoB_2$- and $WB_2$-type are the mix phases among $AlB_2$- and $ReB_2$-type structures. Therefore, the discussions followed are focused more on the $AlB_2$- and $ReB_2$-type structures. The electron transfers from metal to boron atoms, as discussed above, implying an ionic contribution to the M–B bonding. The number of electron transferred from metal to boron atoms decreases from Y to Ag, with the one exception for Rh. This similar behavior concerning the electron transferred from metal to boron atoms is also found in Ref. 9. When combining Table 7 with Fig. 2(d), there is a close correlation in the observed results. When more than (or equal to) one electrons is transferred to B atom for the compounds localized on the left of Mo in the $AlB_2$-type structure, the planar B structure is found to be the energetically preferred. This is confirmed by the synthesis of $YB_2$,[10] $ZrB_2$ (Ref. 11) and $NbB_2$ (Ref. 35) in $AlB_2$-type structure. While less than one electron is transferred to boron atom, the puckered B structure is favored. This is confirmed by the calculated formation enthalpy for $MB_2$ (M = Mo–Ag) and the synthesis of $TcB_2$.[41] The results mentioned above are in agreement with those from the viewpoint of the electro-negativities of metal and boron atoms.[9] For $MoB_2$, there is no obvious preference since there is a very small total energy difference (0.14 eV) between the planar $AlB_2$-type and puckered $ReB_2$-type structures. It is verified by that $MoB_2$ with $MoB_2$- or $WB_2$-type structures

Table 7. Changes in atomic charge as the results of electron transfer from one metal atom to two neighboring boron atoms.

| | $YB_2$ | $ZrB_2$ | $NbB_2$ | $MoB_2$ | $TcB_2$ | $RuB_2$ | $RhB_2$ | $PdB_2$ | $AgB_2$ |
|---|---|---|---|---|---|---|---|---|---|
| | | | | | $ReB_2$-type | | | | |
| $\Delta B$ | −0.43 | −0.42 | −0.40 | −0.37 | −0.34 | −0.33 | −0.43 | −0.31 | −0.16 |
| $\Delta M$ | 0.87 | 0.83 | 0.80 | 0.73 | 0.68 | 0.65 | 0.86 | 0.62 | 0.32 |
| | | | | | $AlB_2$-type | | | | |
| $\Delta B$ | −0.67 | −0.57 | −0.5 | −0.47 | −0.44 | −0.43 | −0.58 | −0.22 | −0.38 |
| $\Delta M$ | 1.34 | 1.15 | 1.06 | 0.95 | 0.89 | 0.86 | 1.16 | 0.45 | 0.76 |
| | | | | | $OsB_2$-type | | | | |
| $\Delta B$ | −0.41 | −0.42 | −0.40 | −0.35 | −0.34 | −0.32 | −0.42 | −0.29 | −0.31 |
| $\Delta M$ | 0.81 | 0.85 | 0.81 | 0.71 | 0.67 | 0.63 | 0.84 | 0.57 | 0.63 |
| | | | | | $MoB_2$-type | | | | |
| $\Delta B_1$ | −0.63 | −0.57 | −0.55 | −0.49 | −0.46 | −0.41 | −0.52 | −0.41 | −0.41 |
| $\Delta B_2$ | −0.45 | −0.45 | −0.41 | −0.39 | −0.34 | −0.31 | −0.31 | −0.23 | −0.32 |
| $\Delta M$ | 1.08 | 1.02 | 0.96 | 0.85 | 0.76 | 0.72 | 0.84 | 0.64 | 0.73 |
| | | | | | $WB_2$-type | | | | |
| $\Delta B_1$ | −0.62 | −0.58 | −0.56 | −0.50 | −0.48 | −0.44 | −0.54 | −0.43 | −0.41 |
| $\Delta B_2$ | −0.45 | −0.45 | −0.54 | −0.48 | −0.44 | −0.40 | −0.50 | −0.38 | −0.32 |
| $\Delta B_3$ | | | −0.41 | −0.36 | −0.34 | −0.31 | −0.31 | −0.23 | |
| $\Delta M$ | 1.08 | 1.02 | 0.96 | 0.85 | 0.80 | 0.73 | 0.83 | 0.64 | 0.73 |



have the smallest formation enthalpy of −1.47 eV (Tables 4 and 5), and their B structures consist of mix phase of planar and puckered sheets. This is confirmed by the synthesized $MoB_2$ in $MoB_2$-type structures.[44]

To get more insight into the bonding mechanism of the different structures, the Mulliken population analysis and bond distances for these diborides are also shown in Fig. 5. The calculated B–B distance in the planar $AlB_2$-type is shorter than that in the puckered one [as shown in Fig. 5(a)], especially the $TcB_2$–$AlB_2$ has the smallest B–B distance about 1.71 Å. As can be seen further from Fig. 5(b), the B–B bond populations are all positive (bonding) and numerically rather large, and the planar $AlB_2$-type have higher B–B bond population values than that in $ReB_2$-type, exception for $ZrB_2$ and $NbB_2$ (both exhibit the same B–B bonding population values to different structure). The results mentioned above support the conclusion that the high degree of B–B covalent bonding exists in all the diborides with both $ReB_2$- and $AlB_2$-type, but which is not enough to guide in explaining the preferential structure formation. From Figs. 5(c) and 5(d), it is also clearly seen that two different bonding characteristics take place in M–B interactions for $ReB_2$-type structure, one is along the *c*-axis (denoted as M–B-I) and the other is in the chains (denoted as M–B-II). It is interesting to note that the bond populations of M–B-II (positive values) are larger than those of M–B-I (negative values) for all the diborides with $ReB_2$-type structure, indicating that M–B-II bonds are stronger than M–B-I bonds. This is in good agreement with the results of the electronic

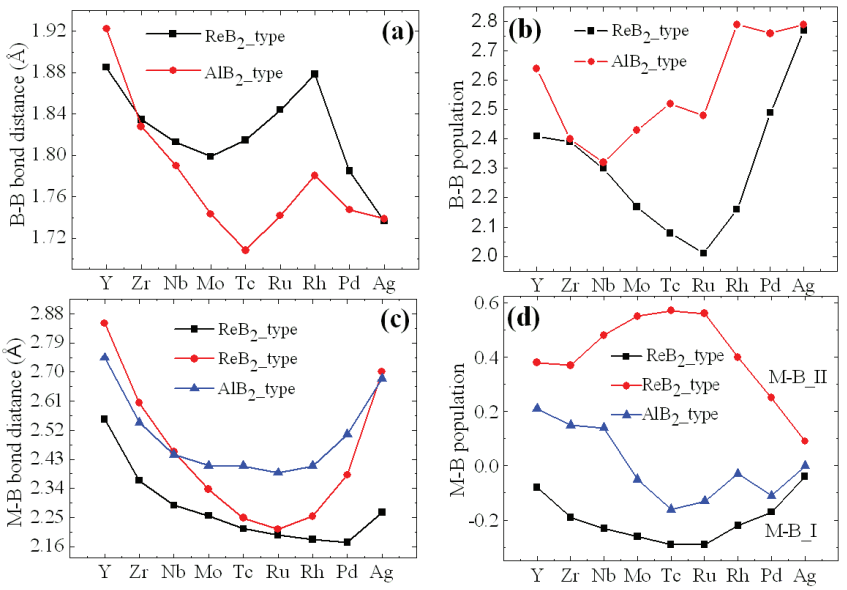


Fig. 5. (Color online) The calculated (a) B–B bond distance (Å), (b) B–B population, (c) M–B bond distance (Å) and (d) M–B population.

localization function (ELF).[8] It may be because the B atoms in the $ReB_2$-type structure do not have inversion symmetry sites, the hexagonal B layers necessarily become nonplanar sheets with B atoms strongly buckled toward the metal atoms that are interconnected by M–B bonds in the chains.[8] For $AlB_2$-type structure, the M–B population is found to be almost zero for Rh and Ag, small and positive for $MB_2$ (M = Y, Zr and Nb) and negative (but also very small) for $MoB_2$, $RuB_2$ and $PdB_2$. The bond population analysis shown in Fig. 5(d) indicates that M–B bonds in the $ReB_2$-type structure are considerable stronger than those in $AlB_2$-type structure. It may be due to that the B atoms in the $AlB_2$-type structure are at sites with inversion symmetry, and the M atom has a higher coordination number (of twelve) than that (of eight) in the $ReB_2$-type structure. This is consistent with the calculated lower $C_{33}$ values in $AlB_2$-type structure (compared with $ReB_2$-type one).

Finally, Poisson's ratio provides more information about the characteristics of bonding force than any of other elastic constants.[47] The value of the Poisson's ratio indicates the degree of directionality of the covalent bonds. The value of the Poisson's ratio is small ($\nu = 0.1$) for covalent materials, whereas for ionic materials a typical value of $\nu$ is about 0.25.[26] From Tables 1–5, it is interesting to see that $ZrB_2$–$AlB_2$ has lowest Poisson's ratio about 0.130 among all the diborides $MB_2$, which suggests that it has the strongest covalent bonding. The Poisson's ratio for both $MoB_2$ and $TcB_2$ in $ReB_2$-type structure is equal to 0.193 and which is the smallest value among diborides $MB_2$ in $ReB_2$-type structure, indicating that they are more directional for both $MoB_2$ and $TcB_2$ with $ReB_2$-type structure. It is worth

to stress that the covalent bonding is more dominant in these compounds, especially for $ZrB_2$–$AlB_2$. While the ionic contribution to the inter-atomic bonding takes more important role in other compounds with higher Poisson's ratio. We thus conclude that the chemical bonding in all the 4d transition-metal diborides is a complex mixture of metallic, ionic and covalent characteristics, and the structural stability of these materials relates mainly on the number of the electrons transferred from metal to boron atoms, boron structure and bond characters.

## 4. Conclusion

The structural stability, elastic, thermodynamic, dynamic and electronic properties of 4d transition-metal diborides $MB_2$ (M = Y to Ag) have been systematically studied by using the first principles calculations based on the DFT with GGA. The calculated formation enthalpy increases from $YB_2$ to $AgB_2$ in $AlB_2$-type structure (similar to $MoB_2$- and $WB_2$-type). While the formation enthalpy decreases from $YB_2$ to $MoB_2$, reaches minimum value to $TcB_2$, and then increases gradually in $ReB_2$-type structure (similar to $OsB_2$-type), which is consistent with the results of the calculated density of states. $MoB_2$ ($ReB_2$-, $OsB_2$-, $MoB_2$- and $WB_2$-type), $TcB_2$ ($ReB_2$- and $OsB_2$-type), $ZrB_2$ ($AlB_2$-type), $NbB_2$ ($AlB_2$-, $MoB_2$- and $WB_2$-type) are the candidates of superhard materials demonstrated by their large shear and bulk moduli, and high Debye temperatures. The calculated results indicate that the boron structure of diborides $MB_2$ is influenced by the electronegative of metals and the number of the electrons transferred from metal to boron atoms. Therefore, diborides $MB_2$ (M = Y, Zr and Nb) favor to induce planar structures, while the diborides $TcB_2$, $RuB_2$, $RhB_2$ and $PdB_2$ are prefer to puckered ones. For $MoB_2$, there is no obvious preference since there is a very small total energy difference (0.14 eV) between the planar $AlB_2$-type and puckered $ReB_2$-type structures. It is confirmed by that $MoB_2$ with $MoB_2$- or $WB_2$-type structures have the smallest formation enthalpy of $-1.47$ eV, and their B structures consist of mix phase of planar and puckered layers. The trend of formation enthalpy is explained by the DOS. The chemical bonding in the 4d transition-metal diborides is a complex mixture of metallic, ionic and covalent characteristics. The strong B–B covalent bonding are dominant for the diborides $MB_2$ in $AlB_2$-type structure, while the M–B (covalent and ionic) bonding is equal important as B–B bonding for the diborides $MB_2$ in $ReB_2$-type one.



## Acknowledgment

The authors thank the National Natural Science Foundation of China for financial support (Grant Nos. 21261013 and 61366008), the Natural Science Foundation of Inner Mongolia Autonomous Region (Grant No. 2011BS0104), the Key Science Research Project of Inner Mongolia University of Technology (Grant No. ZD201117). The authors wish to express thanks to Changchun Institute of Applied Chemistry (Chinese Academy Sciences) for the computer time.

## A.1. Supplementary Materials

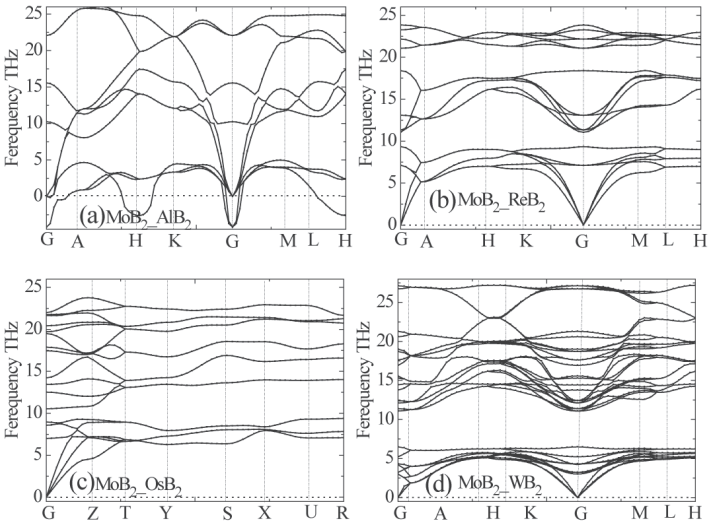


Fig. A.1. The calculated phonon dispersions for $MoB_2$ in the considered structures.

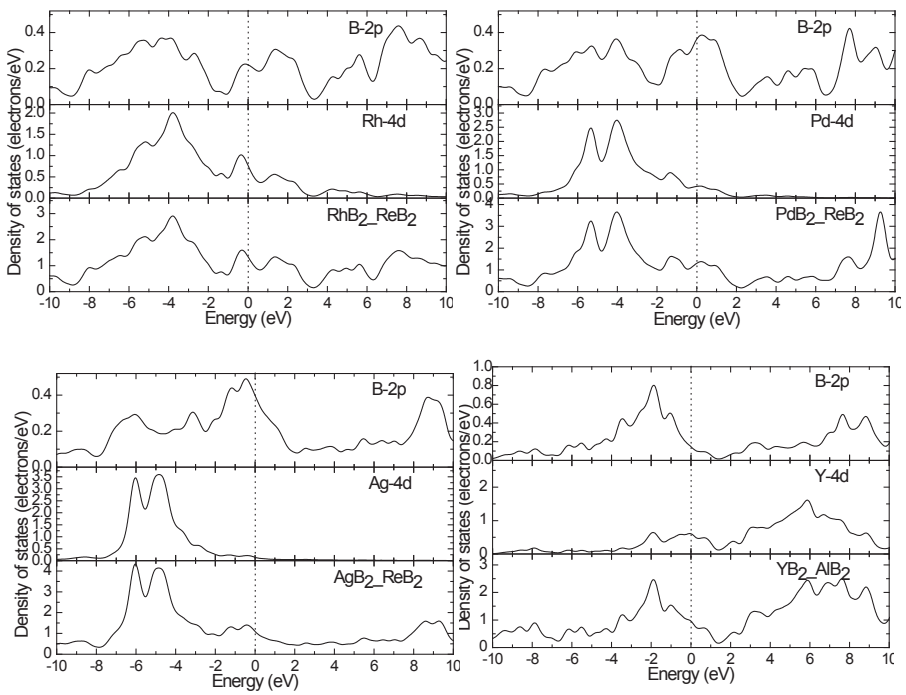


Fig. A.2. Total and partial DOS for 4d transition metal diborides with $AlB_2$ and $ReB_2$ structure at GGA level. The vertical dotted line at zero indicates the Fermi energy level.

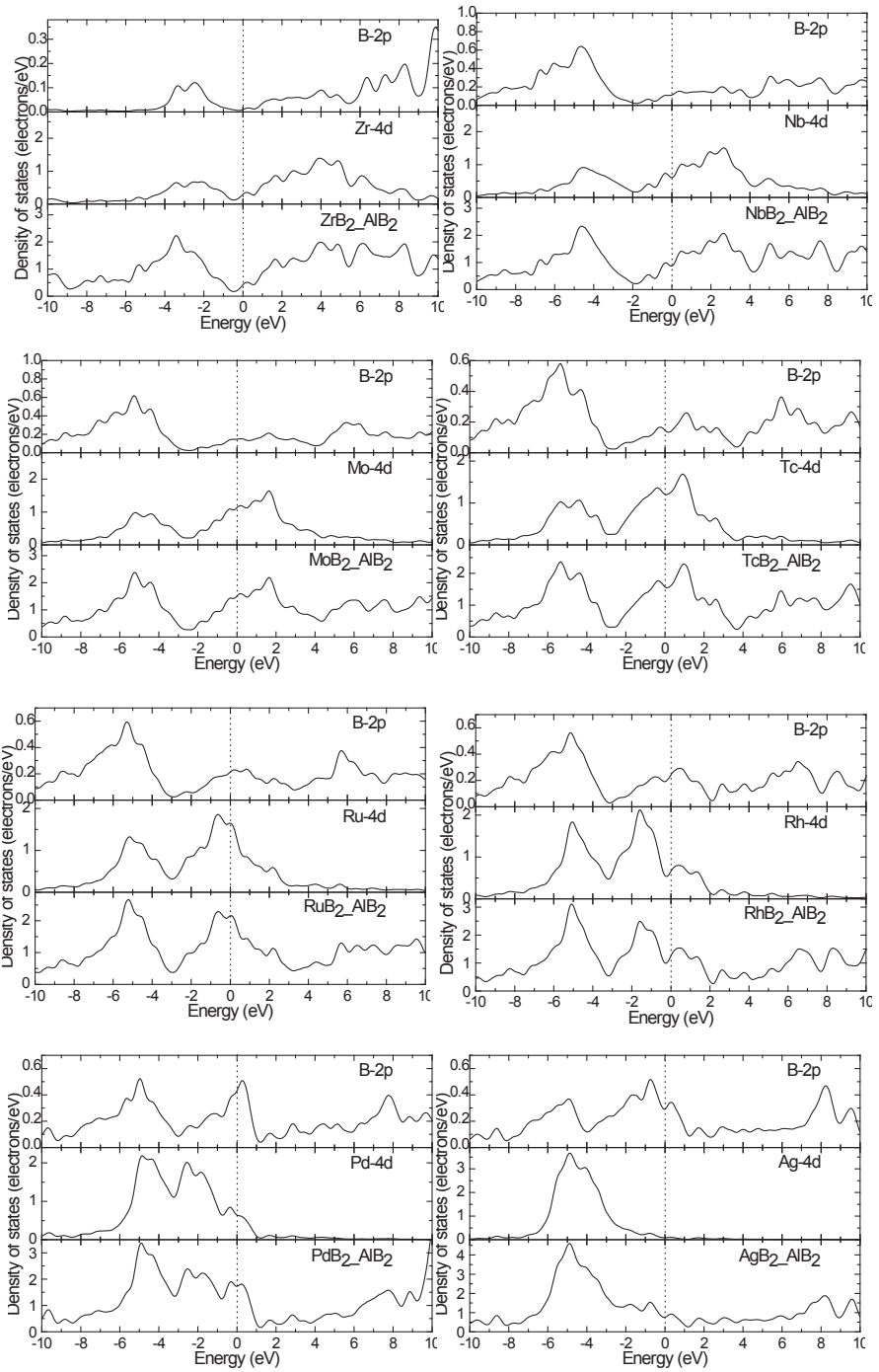


Fig. A.2 (*Continued*)

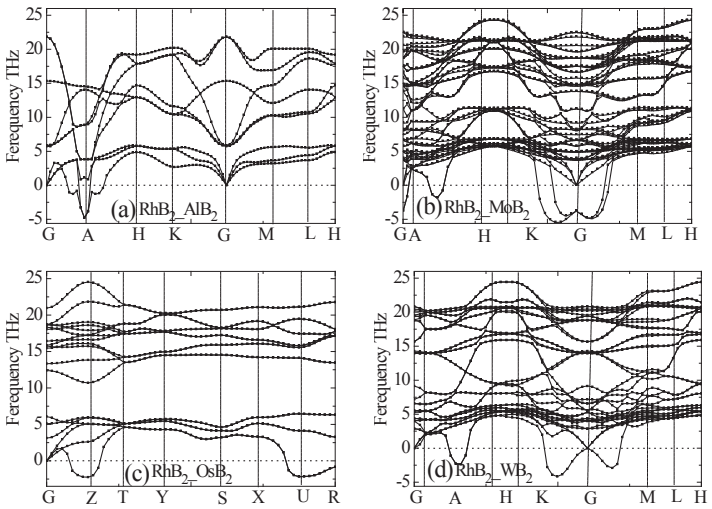


Fig. A.3. The calculated phonon dispersions for $RhB_2$ in the considered structures.



## References

1. Q. Gu, G. Krauss and W. Steurer, *Adv. Mater.* **20** (2008) 3620.
2. E. J. Zhao, J. P. Wang, J. Meng and Z. J. Wu, *Comput. Mater. Sci.* **47** (2010) 1064.
3. H. Y. Chung, M. B. Weinberger, J. B. Levine, A. Kavner, J. M. Yang, S. H. Tolbert and R. B. Kaner, *Science* **316** (2007) 436.
4. E. J. Zhao, J. P. Wang, J. Meng and Z. J. Wu, *J. Comput. Chem.* **31** (2010) 1904.
5. E. J. Zhao, J. Meng, Y. M. Ma and Z. J. Wu, *Phys. Chem. Chem. Phys.* **12** (2010) 13158.
6. R. F. Zhang, S. Veprek and A. S. Argon, *Appl. Phys. Lett.* **91** (2007) 201914.
7. M. Hebbache, L. Stuparević and D. Živković, *Solid State Commun.* **139** (2006) 227.
8. X.-Q. Chen, C. L. Fu, M. Krčmar and G. S. Painter, *Phys. Rev. Lett.* **100** (2008) 196403.
9. A. Pallas and K. Larsson, *J. Phys. Chem. B* **110** (2006) 5367.
10. V. V. Novikov, A. V. Matovnikov, T. A. Chukina, A. A. Sidorov and E. A. Kul'chenkov, *Phys. Solid State* **49** (2007) 2034.
11. S. Ran, O. van der Biest and J. Vleugels, *J. Am. Ceram. Soc.* **93** (2010) 1586.
12. S. Yin, D. He, C. Xu, W. Wang, H. Wang, L. Li, L. Zhang, F. Liu, P. Liu, Z. Wang, C. Meng and W. Zhu, *High Pressure Res.* **33** (2013) 409.
13. H. J. Monkhorst and J. D. Pack, *Phys. Rev. B* **13** (1976) 5188.
14. C. Musa, R. Orru, R. Licheri and G. Cao, *Physica C* **469** (2009) 1991.
15. J. K. Burdett, E. Canadell and G. J. Miller, *J. Am. Chem. Soc.* **108** (1986) 6561.
16. W. Chen and J. Z. Jiang, *Solid State Commun.* **150** (2010) 2093.
17. E. Deligoz, K. Colakoglu and Y. O. Ciftci, *Solid State Commun.* **150** (2010) 405.
18. H. Ihara, M. Hirabayashi and H. Nakagawa, *Phys. Rev. B* **16** (1977) 726.
19. D. L. Johnson, B. N. Harmon and S. H. Liu, *J. Chem. Phys.* **73** (1980) 1898.
20. X. H. Zhang, X. G. Luo, J. C. Han, J. P. Li and W. B. Han, *Comput. Mater. Sci.* **44** (2008) 411.
21. M. G. Zhang, H. Wang, H. B. Wang, T. Cui and Y. M. Ma, *J. Phys. Chem. C* **114** (2010) 6722.

22. S. Chiodo, H. J. Gotsis, N. Russo and E. Sicilia, *Chem. Phys. Lett.* **425** (2006) 311.
23. J. Wang and Y. J. Wang, *J. Appl. Phys.* **105** (2009) 083539.
24. F. Peng, W. M. Peng, H. Z. Fu and X. D. Yang, *Physica B* **404** (2009) 3363.
25. A. Islam, F. Parvin, F. N. Islam, M. N. Islam, A. Islam and I. Tanaka, *Physica C* **466** (2007) 76.
26. H. B. Ozisik, K. Colakoglu and E. Deligoz, *Comput. Mater. Sci.* **51** (2012) 83.
27. L. K. Zhao, E. J. Zhao and Z. J. Wu, *Acta Phys. Sin.* **62** (2013) 046201.
28. M. D. Segall, P. J. D. Lindan, M. J. Probert, C. J. Pickard, P. J. Hasnip, S. J. Clark and M. C. Payne, *J. Phys.: Condens. Matter* **14** (2002) 2717.
29. J. P. Perdew, K. Burke and M. Ernzerhof, *Phys. Rev. Lett.* **77** (1996) 3865.
30. D. Vanderbilt, *Phys. Rev. B* **41** (1990) 7892.
31. W. Voigt, *Lehrbuch der Kristallphysik* (Teubner, Leipzig, 1928).
32. A. Reuss and Z. Angew, *Math. Mech.* **9** (1929) 49.
33. R. Hill, *Proc. Phys. Soc. A* **65** (1952) 349.
34. S. Laplaca and B. Post, *Acta Crystallogr.* **15** (1962) 97.
35. H. Holleck, *J. Nucl. Mater.* **21** (1967) 14.
36. E. Rudy, F. Benesovsky and L. Toth, *Z. Metallkd.* **54** (1963) 345.
37. Z. J. Wu, E. J. Zhao, H. P. Xiang, X. F. Hao, X. J. Liu and J. Meng, *Phys. Rev. B* **76** (2007) 054115.
38. N. L. Okamoto, M. Kusakari, K. Tanaka, H. Inui and S. Otani, *Acta Mater.* **58** (2010) 76.
39. S. F. Pugh, *Philos. Mag.* **45** (1954) 823.
40. W. Trzebiatowski and J. Rudzinski, *J. Alloys Less-Common Met.* **6** (1964) 244.
41. D. M. Teter, *MRS Bull.* **23** (1998) 22.
42. X. Q. Chen, H. Y. Niu, D. Z. Li and Y. Y. Li, *Intermetallics* **19** (2011) 1275.
43. B. Aronsson, *Acta Chem. Scand.* **17** (1963) 2036.
44. I. Higashi, Y. Takahashi and S. Okada, *J. Alloys Less-common Met.* **123** (1986) 277.
45. J. Feng, B. Xiao, R. Zhou, W. Pan and D. R. Clarke, *Acta Mater.* **60** (2012) 3380.
46. P. Ravindran, L. Fast, P. V. Korzhavyi, B. Johansson, J. Wills and O. Eriksson, *J. Appl. Phys.* **84** (1998) 4891.
47. R. Rajeswarapalanichamy, G. S. Priyanga, A. Murugan, M. Santhosh, A. J. Cinthia, S. Kanagaprabha and K. Iyakutti, *J. Alloys Compd.* **580** (2013) 332.